

# Asteroseismological analysis of the ultra-massive ZZ Ceti stars BPM 37093, GD 518, and SDSS J0840+5222

Alejandro H. Córscico<sup>1,2</sup>, Francisco C. De Gerónimo<sup>1,2</sup>, María E. Camisassa<sup>1,2</sup>, Leandro G. Althaus<sup>1,2</sup>

<sup>1</sup>Grupo de Evolución Estelar y Pulsaciones. Facultad de Ciencias Astronómicas y Geofísicas, Universidad Nacional de La Plata, Paseo del Bosque s/n, (1900) La Plata, Argentina

<sup>2</sup>Instituto de Astrofísica La Plata, IALP (CCT La Plata), CONICET-UNLP  
e-mail: acorsico@fcaglp.unlp.edu.ar

Received ; accepted

## ABSTRACT

**Context.** Ultra-massive ( $\geq 1M_{\odot}$ ) hydrogen-rich (DA) white dwarfs are expected to have a substantial portion of their cores in a crystalline state at the effective temperatures characterizing the ZZ Ceti instability strip ( $T_{\text{eff}} \sim 12\,500$  K), as a result of Coulomb interactions in very dense plasmas. Asteroseismological analyses of these white dwarfs can provide valuable information related to the crystallization process, the core chemical composition and the evolutionary origin of these stars.

**Aims.** We present a thorough asteroseismological analysis of the ultra-massive ZZ Ceti star BPM 37093, which exhibits a rich period spectrum, on the basis of a complete set of fully evolutionary models that represent ultra-massive oxygen/neon(ONe)-core DA white dwarf stars harbouring a range of hydrogen (H) envelope thicknesses. We also carry out preliminary asteroseismological inferences on two other ultra-massive ZZ Ceti stars that exhibit fewer periods, GD 518, and SDSS J0840+5222.

**Methods.** We considered *g*-mode adiabatic pulsation periods for ultra-massive ONe-core DA white dwarf models with stellar masses in the range  $1.10 \leq M_{\star}/M_{\odot} \leq 1.29$ , effective temperatures in the range  $10\,000 \leq T_{\text{eff}} \leq 15\,000$  K, and H envelope thicknesses in the interval  $-10 \leq \log(M_{\text{H}}/M_{\star}) \leq -6$ . We explore the effects of employing different H-envelope thicknesses on the mode-trapping properties of our ultra-massive ONe-core DA white dwarf models, and perform period-to-period fits to ultra-massive ZZ Ceti stars with the aim of finding an asteroseismological model for each target star.

**Results.** We found that the trapping cycle and trapping amplitude are larger for thinner H envelopes, and that the asymptotic period spacing is longer for thinner H envelopes. We found a mean period spacing of  $\Delta\Pi \sim 17$  s in the data of BPM 37093, which is likely to be associated to  $\ell = 2$  modes. However, we are not able to put constraints on the stellar mass of BPM 37093 using this mean period spacing due to the simultaneous sensitivity of  $\Delta\Pi$  with  $M_{\star}$ ,  $T_{\text{eff}}$ , and  $M_{\text{H}}$ , an intrinsic property of DAV stars. We found asteroseismological models for the three objects under analysis, two of them (BPM 37093 and GD 518) characterized by canonical (thick) H envelopes, and the third one (SDSS J0840+5222) with a thinner H envelope. The effective temperature and stellar mass of these models are in agreement with the spectroscopic determinations. The percentage of crystallized mass of these asteroseismological models is 92 %, 97 %, and 81 % for BPM 37093, GD 518, and SDSS J0840+5222, respectively. We also derive asteroseismological distances which are in agreement with the astrometric measurements of *Gaia* for these stars.

**Conclusions.** Asteroseismological analyses like the one presented in this paper could lead to a more complete knowledge of the processes occurring during crystallization inside white dwarfs. Also, they could make it possible to deduce the core chemical composition of ultra-massive white dwarfs, and in this way, to infer their evolutionary origin, i.e., if the star has a ONe core and then is the result of single-star evolution, or if it harbour a carbon/oxygen (CO) core and is the product of a merger of the two components of a binary system. However, to achieve these objectives it is necessary to find more pulsating ultra-massive WDs, and also to carry out additional observations of the already known pulsating stars to detect more pulsation periods. Space missions such as *TESS* can give a great boost in this direction.

**Key words.** stars — pulsations — stars: interiors — stars: evolution — stars: white dwarfs

## 1. Introduction

ZZ Ceti (also called DAV stars) stars are the most numerous and best studied class of pulsating white dwarf (WD) stars. They are normal DA WDs with effective temperatures between  $\sim 10\,400$  K and  $\sim 12\,400$  K and logarithm of surface gravities in the range  $[7.5 - 9.1]$ . These stars exhibit brightness variations due to non-radial *g*(gravity) modes with low harmonic degree ( $\ell \leq 2$ ) with periods in the interval  $[70 - 1500]$  s (Winget & Kepler 2008; Fontaine & Brassard 2008; Althaus et al. 2010b; Córscico et al. 2019). The first object of this class, R548, was discovered to be pulsating by Landolt (1968). From then until now, a large number of ZZ Ceti stars have been discovered, initially through specific efforts with observations of bright targets from the ground

(Fontaine & Brassard 2008), then from the Sloan Digital Sky Survey (SDSS; York et al. 2000), and, in the last years, with the *Kepler* space telescope (Borucki 2016), and the *Kepler*'s second mission K2 (Van Cleve et al. 2016). Currently, there are 260 ZZ Ceti stars known (Córscico et al. 2019), and it is expected that the Transiting Exoplanet Survey Satellite (*TESS*; Ricker et al. 2014) will increase this number substantially.

Asteroseismology is a powerful technique that offers the exciting prospect of deducing the internal structure of stars by studying their natural frequencies. In the case of pulsating WDs, the first asteroseismic studies of ZZ Ceti stars that compared the observed periods with the theoretical periods computed on a large grid of realistic DA WD models (the so-called *forward*

method) were carried out by Bradley (1998, 2001). These pioneering works showed that it would be possible, in principle, to infer the internal chemical structure, the stellar mass, surface gravity, effective temperature, luminosity, radius, seismological distance, and rotation rate of ZZ Ceti stars on the basis of the observed pulsation periods. Since then, detailed asteroseismological studies of DAV stars have been carried out, either through the use of fully evolutionary models (Romero et al. 2012, 2013, 2017; De Gerónimo et al. 2017, 2018), or by using static/parametric models (Bischoff-Kim et al. 2008; Fu et al. 2013; Bognár et al. 2016; Giammichele et al. 2017a,b). Both methods have strengths and weaknesses, but eventually they are complementary to each other (see discussion in Córscico et al. 2019).

Of particular interest in this paper is the asteroseismological analysis of the rare ultra-massive ZZ Ceti stars ( $M_{\star} \gtrsim 1M_{\odot}$ ). At variance with average-mass ( $0.50 \lesssim M_{\star}/M_{\odot} \lesssim 0.70$ ) and massive ( $0.70 \lesssim M_{\star}/M_{\odot} \lesssim 1.0$ ) ZZ Ceti stars which likely have C/O cores<sup>1</sup>, ultra-massive ZZ Ceti stars are supposed to harbour cores made mostly of O and Ne if they are the result of single-star evolution. However, it cannot be ruled out that ultra-massive WDs could have CO cores if they are the result of the merger of two WDs (García-Berro et al. 2012). By virtue of their very high masses, these stars are expected to have a large fraction of their cores crystallized at the effective temperatures characterizing the ZZ Ceti instability strip. The crystallization process is due to Coulomb interactions in very dense plasmas. It was theoretically predicted to take place in the cores of WDs six decades ago (Kirzhnits 1960; Abrikosov 1961; Salpeter 1961; van Horn 1968), but it was not until recent times that the existence of crystallized WDs was inferred from the study of WD luminosity function of stellar clusters (Winget et al. 2009; García-Berro et al. 2010), and the galactic field (Tremblay et al. 2019). The effects of crystallization on the pulsational properties of ZZ Ceti star models have been studied by Montgomery & Winget (1999); Metcalfe et al. (2004); Córscico et al. (2004, 2005); Brassard & Fontaine (2005).

In the specific case of ultra-massive WDs with ONe cores, the first attempt of studying their pulsational properties from a theoretical perspective was made by Córscico et al. (2004), who showed that the forward and mean period spacing of ONe-core WDs are markedly different from those of CO-core WDs. Recently, De Gerónimo et al. (2019) revisited the topic by assessing the adiabatic pulsation properties of ultra-massive DA WDs with ONe cores on the basis of a new set of fully evolutionary models generated by Camisassa et al. (2019). These models incorporate the most updated physical ingredients for modelling the progenitor and WD evolution. Specifically, the chemical profiles of the WD models of Camisassa et al. (2019), which were adopted from Siess (2010), are consistent with the predictions of the progenitor evolution with stellar masses in the range  $9.0 < M_{\text{ZAMS}}/M_{\odot} < 10.5$  from the ZAMS to the end of the Super Asymptotic Giant Branch (S-AGB) phase. In addition, these models consider, for the first time, the changes in the core chemical composition resulting from phase separation due to crystallization, according to the predictions of the phase diagram suitable for <sup>16</sup>O and <sup>20</sup>Ne plasma of Medin & Cumming (2010).

In this paper, we perform for the first time a detailed asteroseismological analysis of the ultra-massive ZZ Ceti stars known

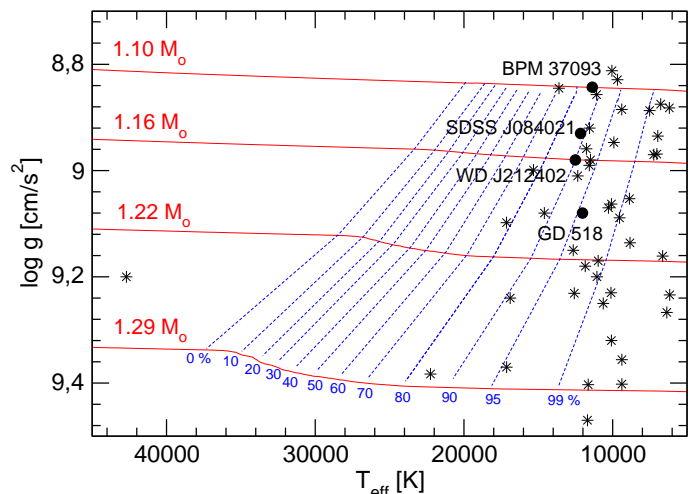


**Fig. 1.** Evolutionary tracks (red solid lines) of the ultra-massive DA WD models computed by Camisassa et al. (2019) in the  $T_{\text{eff}} - \log g$  plane. Blue dashed lines indicate 0, 10, 20, 30, 40, 50, 60, 70, 80, 90, 95 and 99% of crystallized mass. The location of ultra-massive DA WD stars (Kleinman et al. 2013; Kepler et al. 2016; Curd et al. 2017) are indicated with black star symbols. The black circles indicate the location of the known ultra-massive ZZ Ceti stars: BPM 37093 (Nitta et al. 2016), SDSS J084021 (Curd et al. 2017), GD 518 (Hermes et al. 2013), and WD J212402 (Rowan et al. 2019).

up to date on the basis of the new grid of ONe-core WD models presented in Camisassa et al. (2019). At present, there are four objects of this class known: BPM 37093 ( $M_{\star} = 1.1 M_{\odot}$ ; Kanaan et al. 1992), GD 518 ( $M_{\star} = 1.24 M_{\odot}$ ; Hermes et al. 2013), SDSS J084021 ( $M_{\star} = 1.16 M_{\odot}$ ; Curd et al. 2017), and WD J212402 ( $M_{\star} = 1.16 M_{\odot}$ ; Rowan et al. 2019). The location of these stars in the spectroscopic Hertzsprung-Russell (HR) diagram is shown in Fig. 1, along with the evolutionary tracks of Camisassa et al. (2019). The observed pulsation periods of these stars are shown in Tables 1, 3, 5, and 7. The star with the richest pulsation spectrum, BPM 37093 (Table 1), allows for a detailed asteroseismological analysis. This star is the main target in the present paper. The remaining stars exhibit just three periods (GD 518 and SDSS J084021, Tables 3 and 5, respectively) and only one period (WD J212402; Table 7). In view of this, for GD 518 and SDSS J084021 only a preliminary seismological analysis is possible, while for WD J212402 it is not possible at present to carry out any asteroseismological inference. The stellar models on which we base our study consider time-dependent element diffusion and crystallization with chemical rehomogenization due to phase separation. In order to have a set of models suitable for a detailed asteroseismological analysis, we have expanded our set of models by generating new sequences of WD models characterized by H envelopes thinner than the (thick) canonical envelopes. In this way, we extend the parameter space to be explored in our asteroseismological analysis.

The paper is organized as follows. A brief description of the numerical codes and the evolutionary models employed is provided in Sect. 2. In Sect. 3 we present a brief description of the pulsation properties of our models. In Section 4 we perform a detailed asteroseismological analysis of the ultra-massive ZZ Ceti star BPM 37093, and in Section 5 we carry out period-to-period fits to the stars GD 518 and SDSS J084021. Finally, in Sect. 6 we summarize the main findings of this work.

<sup>1</sup> There are also the pulsating Extremely Low-Mass (ELM) and Low-Mass (LM) WDs, also called ELMVs ( $M_{\star} \lesssim 0.30M_{\odot}$ ), which show H-rich atmospheres and are thought to have cores composed by He.

## 2. Numerical codes and evolutionary models

### 2.1. Evolutionary and pulsational codes

The ultra-massive DA WD evolutionary models employed in this work were computed with the LPCODE evolutionary code (see Althaus et al. 2005b, 2010a; Renedo et al. 2010; Miller Bertolami 2016, for detailed physical description). This numerical tool has been employed to study multiple aspects of the evolution of low-mass stars (Wachlin et al. 2011; Althaus et al. 2013, 2015), the formation of horizontal branch stars (Miller Bertolami et al. 2008), extremely low-mass WDs (Althaus et al. 2013), AGB and post-AGB evolution (Miller Bertolami 2016), the evolution of DA WDs (Camisassa et al. 2016) and H-deficient WDs (Camisassa et al. 2017), among others. More recently, the code has been employed to assess the impact of the uncertainties in progenitor evolution on the pulsation properties and asteroseismological models of ZZ Ceti stars (De Gerónimo et al. 2017, 2018). The input physics of the version of the LPCODE evolutionary code employed in this work is described in Camisassa et al. (2019). We refer the interested reader to that paper for details. Of particular importance in this study, is the treatment of crystallization. Theoretical models predict that cool WD stars must crystallize due to the strong Coulomb interactions in their very dense interiors (van Horn 1968). The two additional energy sources induced by crystallization, namely, the release of latent heat, and gravitational energy associated to changes in the chemical profiles induced by crystallization, are consistently taken into account. The chemical redistribution due to phase separation and the associated release of energy have been considered following Althaus et al. (2010c), appropriately modified by Camisassa et al. (2019) for ONe plasmas. To assess the enhancement of  $^{20}\text{Ne}$  in the crystallized core, we used the azeotropic-type phase diagram of Medín & Cumming (2010).

The pulsation code used to compute the nonradial  $g$ -mode pulsations of our complete set of models is the adiabatic version of the LP-PUL pulsation code described in Córscico & Althaus (2006). We did not consider torsional modes, since these modes are characterized by very short periods (up to 20 s; see Montgomery & Winget 1999) which have never been observed in ZZ Ceti stars. To account for the effects of crystallization on the pulsation spectrum of  $g$  modes, we adopted the “hard-sphere” boundary conditions (Montgomery & Winget 1999; Córscico et al. 2005), which assume that the amplitude of the radial displacement of  $g$  modes is drastically reduced below the solid/liquid boundary layer because of the non-shear modulus of the solid, as compared with the amplitude in the fluid region (Montgomery & Winget 1999). The squared Brunt-Väisälä frequency ( $N^2$ ) for the fluid part of the models is computed as in Tassoul et al. (1990). The Ledoux term  $B$ , that explicitly contains the contributions of the chemical interfaces to the Brunt-Väisälä frequency, has been appropriately generalized in order to include the presence of transition regions in which multiple nuclear species vary in abundance.

### 2.2. The grid of ultra-massive ONe-core WD models

The asteroseismological analysis presented in this work is based on a set of four evolutionary sequences of ultra-massive WD models with stellar masses  $M_\star = 1.10, 1.16, 1.22,$  and  $1.29 M_\odot$  resulting from the complete evolution of the progenitor stars through the S-AGB phase (Camisassa et al. 2019). The core and inter-shell chemical profiles of our models at the start of the

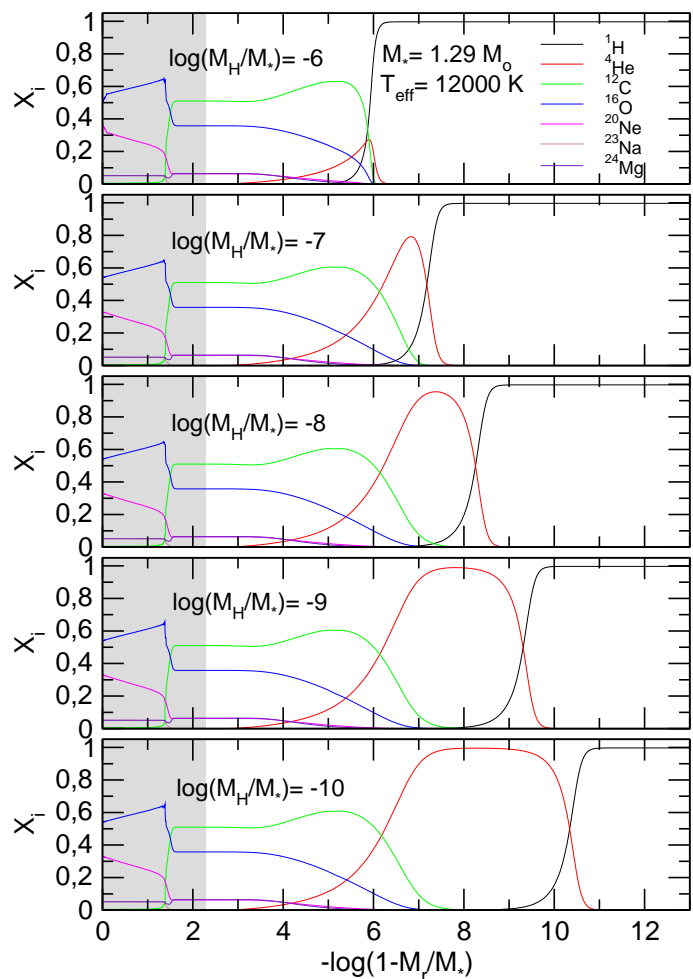


**Fig. 2.** Abundances by mass of  $^1\text{H}$ ,  $^4\text{He}$ ,  $^{12}\text{C}$ ,  $^{16}\text{O}$ ,  $^{20}\text{Ne}$ ,  $^{23}\text{Na}$ , and  $^{24}\text{Mg}$  as a function of the fractional mass, corresponding to ONe-core WD models with  $M_\star 1.29 M_\odot$ ,  $T_{\text{eff}} \sim 12000$  K and  $\log(M_{\text{H}}/M_\star) = -6, -7, -8, -9,$  and  $-10$  (from top to bottom). The models were computed taking into account time-dependent element diffusion, and latent heat release and chemical redistribution caused by phase separation during crystallization. The solid part of the models is emphasized with a gray tone. The crystallized mass fraction (in percentage) is 99.5%.

WD cooling phase were derived from Siess (2010). The cores are composed mostly of  $^{16}\text{O}$  and  $^{20}\text{Ne}$  and smaller amounts of  $^{12}\text{C}$ ,  $^{23}\text{Na}$ , and  $^{24}\text{Mg}$  (see Figs. 2 and 3 of Camisassa et al. 2019). Since element diffusion and gravitational settling operate throughout the WD evolution, our models develop pure H envelopes. The He content of our WD sequences is given by the evolutionary history of progenitor star, but instead, the H content of our canonical (thick) envelopes [ $\log(M_{\text{H}}/M_\star) \sim -6$ ] has been set by imposing that the further evolution does not lead to H thermonuclear flashes on the WD cooling track. We have expanded our grid of models by artificially generating new sequences harbouring thinner H envelopes [ $\log(M_{\text{H}}/M_\star) = -7, -8, -9, -10$ ], for each stellar-mass value. This artificial procedure has been done at high-luminosity stages of the WD evolution. The resulting transitory effects of this procedure become irrelevant much before the models reach the ZZ Ceti regime. Details about the method to compute the chemical rehomogenization at the core regions during crystallization are given in Camisassa et al. (2019) and De Gerónimo et al. (2019). The temporal changes of the chemical abundances due to element diffusion are assessed by using a new full-implicit treatment for time-dependent ele-

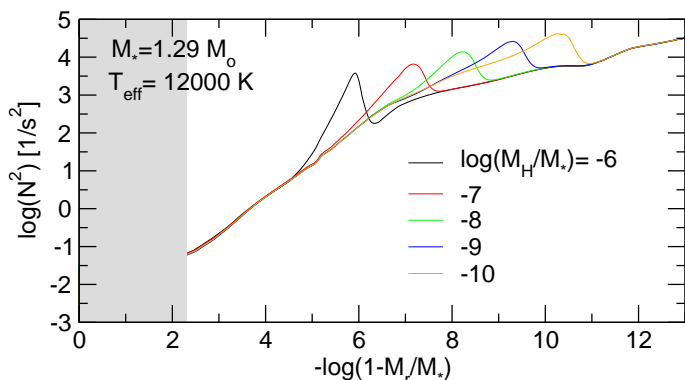


**Fig. 3.** Logarithm of the squared Brunt-Väisälä frequency, corresponding to the same ONe-core WD models with  $M_\star = 1.29M_\odot$ ,  $T_{\text{eff}} \sim 12000$  K and  $\log(M_{\text{H}}/M_\star) = -6, -7, -8, -9$ , and  $-10$  shown in Fig. 2. They gray zone corresponds to the crystallized part of the models.

ment diffusion described in detail in Althaus et al. (2019, submitted).

In Fig. 2 we show the  $^1\text{H}$ ,  $^4\text{He}$ ,  $^{12}\text{C}$ ,  $^{16}\text{O}$ ,  $^{20}\text{Ne}$ ,  $^{23}\text{Na}$ , and  $^{24}\text{Mg}$  chemical profiles in terms of the fractional mass for  $1.29M_\odot$  ONe-core WD models at  $T_{\text{eff}} \sim 12000$  K and H envelope thicknesses  $\log(M_{\text{H}}/M_\star) = -6, -7, -8, -9$ , and  $-10$ . Note that a pure He buffer develops as we consider thinner H envelopes (from the top to the bottom panel).

At this effective temperature, the chemical rehomogenization due to crystallization has already finished, giving rise to a core where the abundance of  $^{16}\text{O}$  ( $^{20}\text{Ne}$ ) increases (decreases) outward. In Fig. 3 we show the logarithm of the squared Brunt-Väisälä frequency corresponding to the same models shown in Fig. 2. The step at the triple chemical transition between  $^{12}\text{C}$ ,  $^{16}\text{O}$ , and  $^{20}\text{Ne}$  seen in Fig. 2 [ $-\log(1 - M_r/M_\star) \sim 1.4$ ] is within the solid part of the core, thus, it is irrelevant for the mode-trapping properties of these models. This is because, according to the hard-sphere boundary conditions adopted for the pulsations, the eigenfunctions do not penetrate the solid region (gray zone). In view of this, the mode-trapping properties of the models illustrated in Fig. 2 and 3 are entirely determined by the presence of the He/H transition and the associated bump in the Brunt-Väisälä frequency, which is located in more external regions for thinner H envelopes (see the next Section).

### 3. Pulsation calculations

We computed adiabatic pulsation periods of  $\ell = 1, 2$   $g$  modes in a range of periods covering the period spectrum that is typically observed in ZZ Ceti stars ( $70 \text{ s} \lesssim \Pi \lesssim 1500 \text{ s}$ ). We briefly examine the impact of the inclusion of thin H envelopes on the mode-trapping properties of our ultra-massive WD models. Mode trapping of  $g$  modes in WDs is a well-studied mechanical resonance for the mode propagation, that acts due to the presence of density gradients induced by chemical transition regions. Specifically, chemical transition regions, which involve non-negligible jumps in density, act like reflecting walls that partially trap certain modes, forcing them to oscillate with larger amplitudes in specific regions and with smaller amplitudes outside those regions (see, for details, Brassard et al. 1992a,b; Bradley et al. 1993; Córscico et al. 2002). From an observational point of view, a possible signature of mode trapping in a WD star is the departure from uniform period spacing. According to the asymptotic theory of stellar pulsations, *in absence of chemical gradients*, the pulsation periods of  $g$  modes with high radial

order  $k$  (long periods) are expected to be uniformly spaced with a constant period separation given by (Tassoul et al. 1990):

$$\Delta\Pi_\ell^a = \Pi_0 / \sqrt{\ell(\ell + 1)}, \quad (1)$$

where

$$\Pi_0 = 2\pi^2 \left[ \int_{\text{fluid}} \frac{N}{r} dr \right]^{-1}. \quad (2)$$

Actually, the period separation in *chemically stratified* WD models like the ones considered in this work is not constant, except for very-high radial-order modes. We define the forward period spacing as  $\Delta\Pi_k = \Pi_{k+1} - \Pi_k$ . The left panels of Fig. 4 show  $\Pi_k - \Delta\Pi_k$  diagrams for the same WD models depicted in Figs. 2 and 3. These models are characterized by  $M_\star = 1.29M_\odot$  at  $T_{\text{eff}} \sim 12500$  K, and different thicknesses of the H envelope. In each panel, the horizontal dashed line corresponds to the asymptotic period spacing, computed with Eqs. (1) and (2). Models with decreasing H envelope thicknesses are displayed from top to bottom, starting with the case of the canonical envelope. By examining the plots, several aspects are worth mentioning. Firstly, the asymptotic period spacing increases for decreasing H envelope thickness. This is because the integral in Eq. (2) for the quantity  $\Pi_0$  is smaller for thinner H envelopes, by virtue that the bump in the Brunt-Väisälä frequency induced by the He/H chemical interface becomes progressively narrow in the radial coordinate  $r$  as this interface is located at more external layers. Since  $\Pi_0$  is larger for thinner H envelopes, the asymptotic period spacing increases (Eq. 1).  $\Delta\Pi_\ell^a$  experiences an increase between 37% and 60% when we go from the canonical envelope [ $\log(M_{\text{H}}/M_\star) = -6$ ] to the thinnest envelope [ $\log(M_{\text{H}}/M_\star) = -10$ ] for this sequence. Other outstanding feature to be noted from the left panels of Fig. 4 is connected with the changes in the mode-trapping properties when we consider H envelopes progressively thinner. Indeed, we note that for thick envelopes, including the canonical one, the period-spacing distribution of  $g$  modes shows a regular pattern of mode trapping with a very short trapping cycle—the  $k$  interval between two trapped modes. When we consider thinner H envelopes, the trapping cycle and the trapping amplitude increase. A common feature for all the values of  $\log(M_{\text{H}}/M_\star)$  considered is that the mode-trapping signatures exhibited by  $\Delta\Pi_k$  vanish for very large radial orders (very long periods), in which case  $\Delta\Pi_k$  approaches to  $\Delta\Pi_\ell^a$ , as predicted by the asymptotic theory.

Mode-trapping effects also translate into local maxima and minima in the kinetic energy of oscillation,  $E_{\text{kin}}$ , which are usually associated to modes that are partially confined to the core regions and modes that are partially trapped in the envelope. This can be appreciated in the right panels of Fig. 4. The behaviour described above for  $\Delta\Pi_k$  is also found in the case of  $E_{\text{kin}}$ , that is, the mode-trapping cycle and amplitude increase with decreasing H envelope thickness.

### 4. Asteroseismological analysis of BPM 37093

Kanaan et al. (1992) discovered the first ultra-massive ZZ Ceti star, BPM 37093. This star is characterized by  $T_{\text{eff}} = 11370$  K and  $\log g = 8.843$  (Nitta et al. 2016). Detailed theoretical computations carried out by Winget et al. (1997), Montgomery (1998), and Montgomery & Winget (1999), suggested that BPM 37093 should have a crystallized core. This star has been the target of two multisite observing campaigns of the Whole

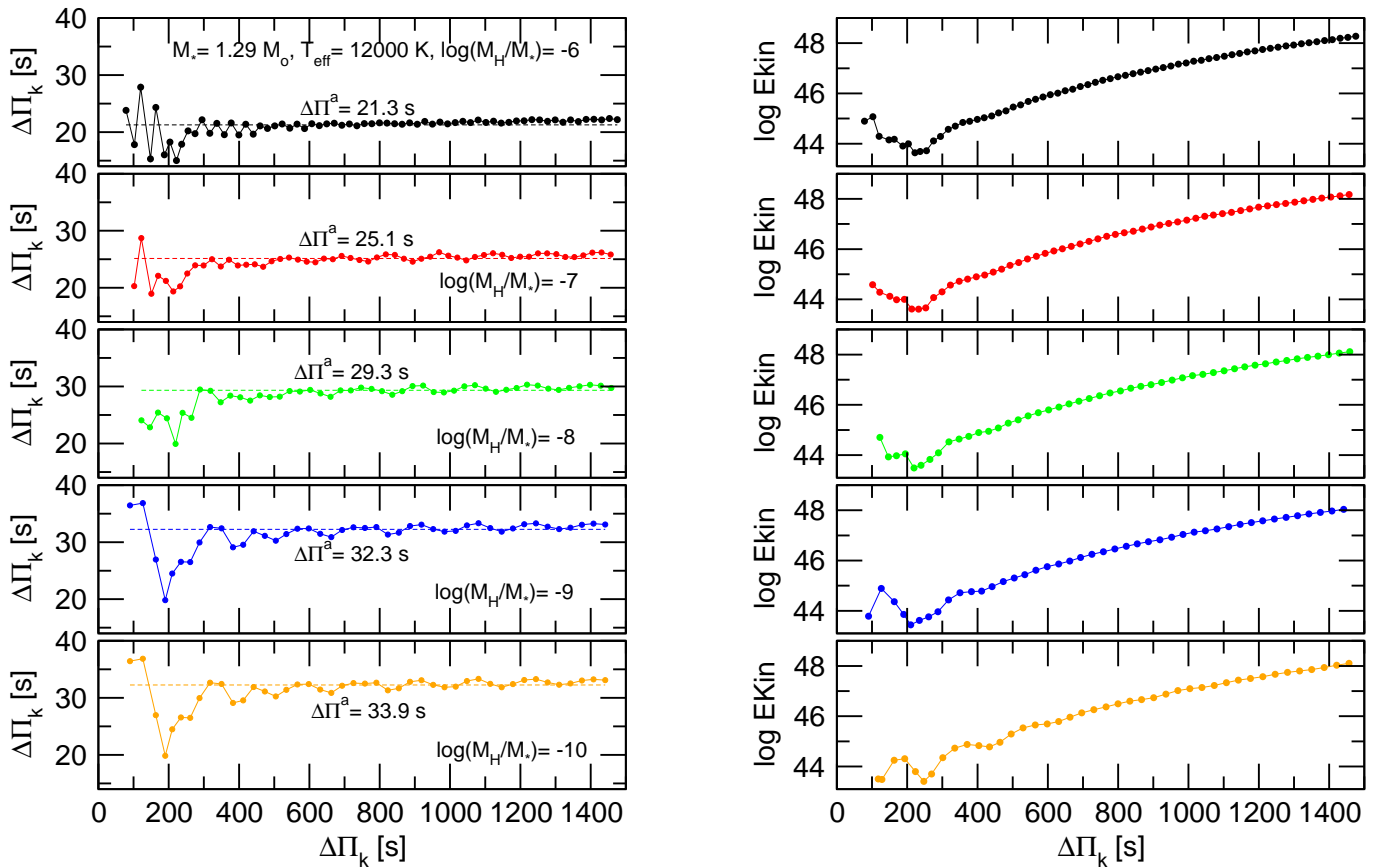


**Fig. 4.** Left panels: the forward period spacing,  $\Delta\Pi_k$ , in terms of the pulsation periods,  $\Pi_k$ , for WD models with  $M_* = 1.29 M_\odot$ ,  $T_{\text{eff}} \sim 12000$  K and different thicknesses of the H envelope. The thin horizontal dashed lines correspond to the value of the asymptotic period spacing  $\Delta\Pi^a$ . Right panels: the oscillation kinetic energy versus the periods for the same WD (being the radial displacement), has been assumed to compute the kinetic energy.

Earth Telescope (WET; Nather et al. 1990). Preliminary results from these campaigns were published by Kanaan et al. (2000). The 1998 observations (XCov 16) revealed a set of regularly spaced pulsation frequencies in the range  $1500\text{--}2000 \mu\text{Hz}$ . The 1999 observations (XCov 17) revealed a total of four independent modes, including two new modes and two that had been seen in the previous campaign. By comparing pulsation amplitudes in the UV to the optical spectra, Nitta (2000) identified the harmonic degree of the BPM 37093 pulsation modes, concluding that they can not be  $\ell = 3$  and that most of the modes must be  $\ell = 2$ . Metcalfe et al. (2004) obtained new single-site observations of BPM 37093 from the Magellan 6.5 m telescope on three nights in 2003 February. These data showed evidence of five independent modes, all of which had been detected in the two previous multisite campaigns. Kanaan et al. (2005) reported on WET observations of BPM 37093 obtained in 1998 and 1999 and, on the basis of a simple analysis of the average period spacing, they concluded that a large fraction of the total stellar mass of the star should be crystallized. On the basis of asteroseismological techniques, Metcalfe et al. (2004) reported to have "measured" the crystallized mass fraction in BPM 37093 and determined a value  $\sim 90\%$ . However, employing similar asteroseismological methods, Brassard & Fontaine (2005) questioned those conclusions, suggesting instead that the percentage of crystallized mass of BPM 37093 probably should be between  $32\%$  and  $82\%$ . In the next sections, we carry out a detailed asteroseismological analysis that involves the assessment of a mean period spacing and its comparison with the theoretical values,

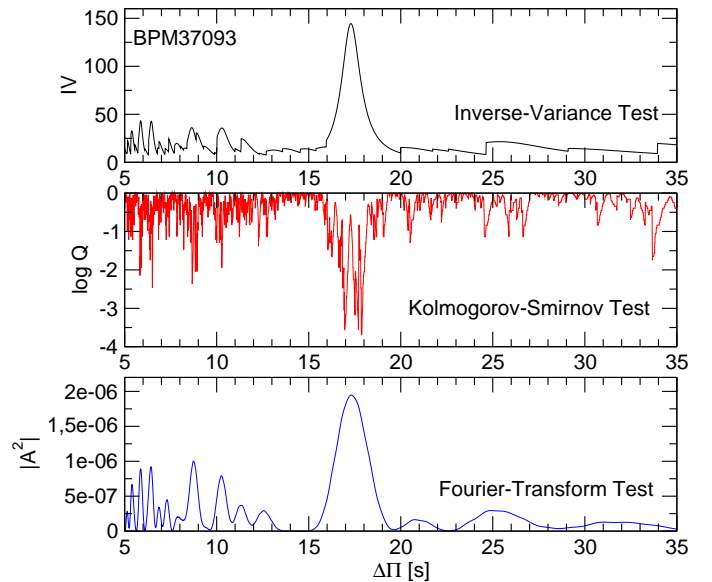


**Fig. 5.** I-V (upper panel), K-S (middle panel), and F-T (bottom panel) significance tests applied to the period spectrum of BPM 37093 to search for a constant period spacing. The periods used here are the 8 periods shown in Table 1.

and also period-to-period fits with the intention of finding an asteroseismological model.

**Table 1.** The independent frequencies and periods in the data of BPM 37093 from Metcalfe et al. (2004), along with the theoretical periods, harmonic degrees, radial orders, and period differences of the best-fit model described in Sect. 4.3.

$\Pi^O$	$\nu$	$\Pi^T$	$\ell$	$k$	$\delta_i$
[sec]	[ $\mu$ Hz]	[sec]			[sec]
511.7	1954.1	512.4	2	29	-0.7
531.1	1882.9	531.9	1	17	-0.8
548.4	1823.5	548.1	2	31	0.3
564.1	1772.7	565.3	2	32	-1.2
582.0	1718.2	583.0	2	33	-1.0
600.7	1664.9	599.9	2	34	0.8
613.5	1629.9	613.8	1	20	-0.3
635.1	1574.6	632.2	2	36	2.9

#### 4.1. Period spacing

For the asteroseismological analysis of this star, we adopt the set of eight modes considered by Metcalfe et al. (2004) (see Table 1). This list of periods is based on the set of periods detected by Nitta (2000). We searched for a constant period spacing in the data of BPM 37093 by using the Kolmogorov-Smirnov (K-S; see Kawaler 1988), the inverse variance (I-V; see O’Donoghue 1994) and the Fourier Transform (F-T; see Handler et al. 1997) significance tests. In the K-S test, any uniform or at least systematically non-random period spacing in the period spectrum of the star will appear as a minimum in  $Q$ . In the I-V test, a maximum of the inverse variance will indicate a constant period spacing. Finally, in the F-T test, we calculate the Fourier transform of a Dirac comb function (created from the set of observed periods), and then we plot the square of the amplitude of the resulting function in terms of the inverse of the frequency. And once again, a maximum in the square of the amplitude will indicate a constant period spacing. In Fig. 5 we show the results of applying the tests to the set of periods of Table 1. The three tests indicate the existence of a mean period spacing of about 17 s. According to our set of models, the asymptotic period spacing (Eq. 1) for ultra-massive DA WDs with masses between 1.10 and 1.29 $M_\odot$  and effective temperatures within the ZZ Ceti instability strip (13 500K – 10 500 K) varies between  $\sim 22$  s and  $\sim 34$  s for  $\ell = 1$ , and between  $\sim 12$  s and  $\sim 19$  s for  $\ell = 2$ . Clearly, the period spacing evidenced by the 3 tests for BPM 37093 corresponds to modes  $\ell = 2$ . This indicates that the period spectrum of this star is dominated by quadrupole modes, being this in concordance with the finding of Nitta (2000). By averaging the period spacing derived from the three statistical tests, we found  $\Delta\Pi_{\ell=2} = 17.3 \pm 0.9$  s.

Nitta et al. (2016) expanded the set of periods of Nitta (2000) for BPM 37093 by employing Gemini South time-series combined with simultaneous time-series photometry from Mt. John (New Zealand), SAAO, PROMPT, and Complejo Astronómico El Leoncito (CASLEO, Argentina), providing a list of 13 periods (see their Table 1). Averaging two pairs of periods, the list gives 11 periods, of which 8 are the same as in Metcalfe et al. (2004), and the remaining 3 periods are new periods with values 624.2 s, 641.0 s, 660.8 s. We have applied the three statistical tests to this expanded list of periods, but we have not found a clear period spacing. This is because the 3 new periods do not fit well into the regular pattern of periods with  $\ell = 2$  shown in Table 1.

#### 4.2. Average of the computed period spacings

In principle, the stellar mass of pulsating WDs can be derived by comparing the average of the period spacings (or the asymptotic period spacing<sup>2</sup>) computed from a grid of models with different masses, effective temperatures, and envelope thicknesses with the mean period spacing exhibited by the star, if present. This method takes full advantage of the fact that the period spacing of DBV (pulsating DB WDs) and GW Vir stars (pulsating PG1159 stars) primarily depends on the stellar mass and the effective temperature, and very weakly on the thickness of the He envelope in the case of DBVs (see, e.g., Tassoul et al. 1990) and the thickness of the C/O/He envelope in the case of the GW Vir stars (Kawaler & Bradley 1994). In the case of ZZ Ceti stars, however, the the average of the period spacings and the asymptotic period spacing depend on the stellar mass, the effective temperature, and the thickness of the H envelope with a comparable sensitivity. Consequently, the method is not –in principle– directly applicable to ZZ Ceti stars due to the intrinsic degeneracy of the dependence of  $\Delta\Pi$  with the three parameters  $M_\star$ ,  $T_{\text{eff}}$ , and  $M_{\text{H}}$  (Fontaine & Brassard 2008).

In spite of this caveat, we tried to derive the stellar mass of BPM 37093 from the measured quadrupole period spacing. To this end, we assessed the average quadrupole period spacings computed for our models as  $\overline{\Delta\Pi}_{\ell=2} = (n - 1)^{-1} \sum_k^n \Delta\Pi_k$ , where  $\Delta\Pi_k$  is the forward period spacing for  $\ell = 2$  modes and  $n$  is the number of theoretical periods considered from the model. For BPM 37093, the observed periods are in the range [511, 635] s. In computing the averaged period spacings for the models, however, we have considered the range [500, 1400] s, that is, we adopted a longer upper limit of this range of periods in order to better sample the period spacing of modes within the asymptotic regime. In Fig. 6 we show the run of the average of the computed period spacings ( $\ell = 2$ ) in terms of the effective temperature for our ultra-massive DA WD evolutionary sequences for all the thicknesses of the H envelope, along with the observed period spacing for BPM 37093. As can be appreciated from the figure, it is not possible in this instance to put very strong constraints on the mass of BPM 37093, and the only thing that can be assured is that the mass of the star could be  $M_\star = 1.16M_\odot$  with a thick (canonical) H envelope [ $\log(M_{\text{H}}/M_\star) = -6$ ], but it could also be as massive as  $M_\star = 1.29M_\odot$  and with a H envelope 100 times thinner [ $\log(M_{\text{H}}/M_\star) = -8$ ]. This degeneracy of the solutions could be eliminated with the help of period-to-period fits. In the next section, we address this issue.

#### 4.3. Period-to-period fits

Here, we search for a pulsation model that best matches the *individual* pulsation periods of BPM 37093. The goodness of the match between the theoretical pulsation periods ( $\Pi_k^T$ ) and the observed individual periods ( $\Pi_i^O$ ) is measured by means of a merit function defined as:

$$\chi^2(M_\star, M_{\text{H}}, T_{\text{eff}}) = \frac{1}{N} \sum_{i=1}^N \min[(\Pi_i^O - \Pi_k^T)^2], \quad (3)$$

<sup>2</sup> Generally, the use of the asymptotic period spacing (computed according to Eq. 1), instead of the average of the computed period spacings, can lead to an overestimation of the stellar mass, except for stars that pulsate with very high radial orders, such as PNNV stars (Althaus et al. 2008).

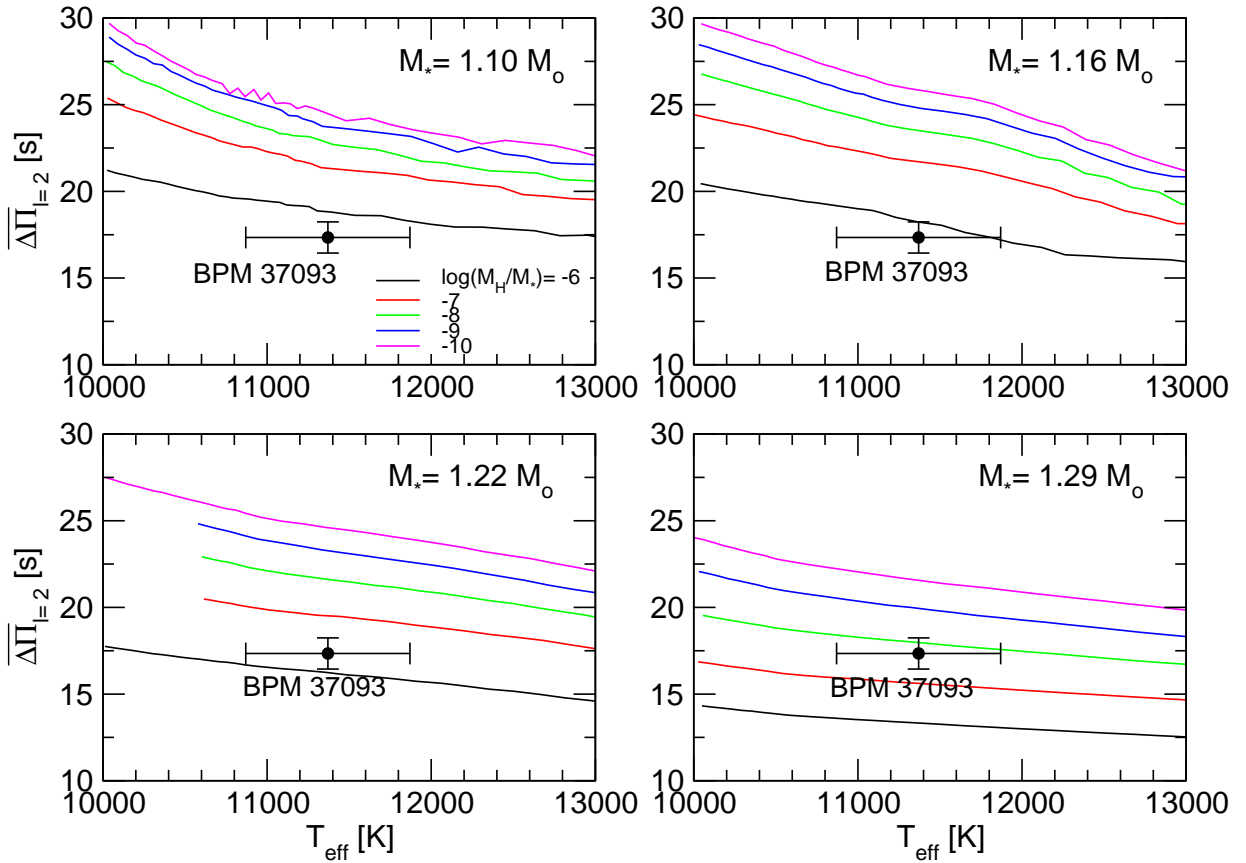


**Fig. 6.** Comparison between the quadrupole ( $\ell = 2$ ) period spacing derived for BPM 37093 ( $\Delta\Pi = 17.3 \pm 0.9$  s), and the average of the computed  $\ell = 2$  period spacings,  $\overline{\Delta\Pi}_{\ell=2}$ , for all the considered stellar masses and different H-envelope thicknesses, in terms of the effective temperature.

where  $N$  is the number of observed periods. The WD model that shows the lowest value of  $\chi^2$ , if exists, is adopted as the “best-fit model”. We assess the function  $\chi^2 = \chi^2(M_*, M_H, T_{\text{eff}})$  for stellar masses of 1.10, 1.16, 1.22, and 1.29  $M_\odot$ . For the effective temperature we cover a range of  $15000 \gtrsim T_{\text{eff}} \gtrsim 10000$  K. Finally, for the H-envelope thickness we adopt the values  $\log(M_H/M_*) = -6, -7, -8, -9, -10$ . The quality of our period fits is assessed by means of the average of the absolute period differences,  $\bar{\delta} = (\sum_{i=1}^N |\delta_i|)/N$ , where  $\delta_i = \Pi_i^O - \Pi_k^T$ , and by the root-mean-square residual,  $\sigma = \sqrt{(\sum_{i=1}^N |\delta_i|^2)/N} = \sqrt{\chi^2}$ .

We assumed two possibilities for the mode identification: (i) that all of the observed periods correspond to  $g$  modes associated to  $\ell = 1$ , and (ii) that the observed periods correspond to a mix of  $g$  modes associated to  $\ell = 1$  and  $\ell = 2$ . We first considered the 8 periods employed by Metcalfe et al. (2004) (see Table 1). The case (i) did not show clear solutions compatible with BPM 37093 in relation to its spectroscopically-derived effective temperature. Instead, the case (ii), in which we allow the periods of the star to be associated to a combination of  $\ell = 1$  and  $\ell = 2$  modes, resulted in a clear seismological solution for a WD model with  $M_* = 1.16 M_\odot$ ,  $T_{\text{eff}} = 11\,650$  K and  $\log(M_H/M_*) = -6$ , as it can be appreciated from Fig. 7. In Table 1 we show the periods of the best-fit model along with the harmonic degree, the radial order, and the period differences. For this model, we obtain  $\bar{\delta} = 1.00$  s and  $\sigma = 1.28$  s. In order to have an indicator of the quality of the period fit, we computed the Bayes Information Criterion (BIC;

Koen & Laney 2000):

$$\text{BIC} = N_p \left( \frac{\log N}{N} \right) + \log \sigma^2, \quad (4)$$

where  $N_p$  is the number of free parameters of the models, and  $N$  is the number of observed periods. The smaller the value of BIC, the better the quality of the fit. In our case,  $N_p = 3$  (stellar mass, effective temperature, and thickness of the H envelope),  $N = 8$ , and  $\sigma = 1.28$  s. We obtain BIC = 0.55, which means that our fit is very good. In Table 2, we list the main characteristics of the best-fit model. The seismological stellar mass is in good agreement with the spectroscopic inference based on the evolutionary tracks of Camisassa et al. (2019). The quadrupole ( $\ell = 2$ ) mean period spacing of our best fit model is  $\overline{\Delta\Pi} = 17.63$  s, in excellent agreement with the mean period spacing derived for BPM 37093 ( $\Delta\Pi = 17.3 \pm 0.9$  s). Fig. 8 depicts the chemical profiles (upper panel) and the propagation diagram (lower panel) corresponding to the best-fit model of BPM 37093. Our best-fit model has  $\sim 92\%$  of its mass in crystalline state.

We repeated the process of period fit considering the preliminary set of 13 periods observed by Nitta et al. (2016), but we did not find a clear seismological solution neither when we considered the case (i) nor when we adopted the case (ii).

#### 4.4. Internal uncertainties

We have assessed the uncertainties in the stellar mass ( $\sigma_{M_*}$ ), the thickness of the H envelope ( $\sigma_{M_H}$ ), and the effective tempera-

**Table 2.** The main characteristics of BPM 37093. The second column corresponds to spectroscopic and astrometric results, whereas the third column presents results from the asteroseismological model of this work.

Quantity	Spectroscopy	Asteroseismology
$T_{\text{eff}}$ [K]	$11\,370 \pm 500^{(a)}$	$11\,650 \pm 40$
$M_{\star}/M_{\odot}$	$1.098 \pm 0.1^{(b)}$	$1.16 \pm 0.014$
$\log g$ [cm/s <sup>2</sup> ]	$8.843 \pm 0.05^{(a)}$	$8.970 \pm 0.025$
$\log(L_{\star}/L_{\odot})$	—	$-3.25 \pm 0.01$
$\log(R_{\star}/R_{\odot})$	—	$-2.234 \pm 0.006$
$\log(M_{\text{H}}/M_{\star})$	—	$-6 \pm 0.26$
$\log(M_{\text{He}}/M_{\star})$	—	$-3.8$
$M_{\text{cr}}/M_{\star}$	$0.935^{(b)}$	$0.923$
$X_{16\text{O}}$ cent.	—	$0.52$
$X_{20\text{Ne}}$ cent.	—	$0.34$
Quantity	Measured	Asteroseismology
$\Delta\Pi_{\ell=1}$ [s]	—	$29.70$
$\Delta\Pi_{\ell=2}$ [s]	$17.3 \pm 0.9$	$17.63$
Quantity	Astrometry ( <i>Gaia</i> )	Asteroseismology
$d$ [pc]	$14.81 \pm 0.01$	$11.38 \pm 0.06$
$\pi$ [mas]	$67.52 \pm 0.04$	$87.87 \pm 0.40$

References: (a) Nitta et al. (2016). (b) Camisassa et al. (2019)

ture ( $\sigma_{T_{\text{eff}}}$ ), of the best-fit model by employing the expression (Zhang et al. 1986; Castanheira & Kepler 2008):

$$\sigma_i^2 = \frac{d_i^2}{(S - S_0)}, \quad (5)$$

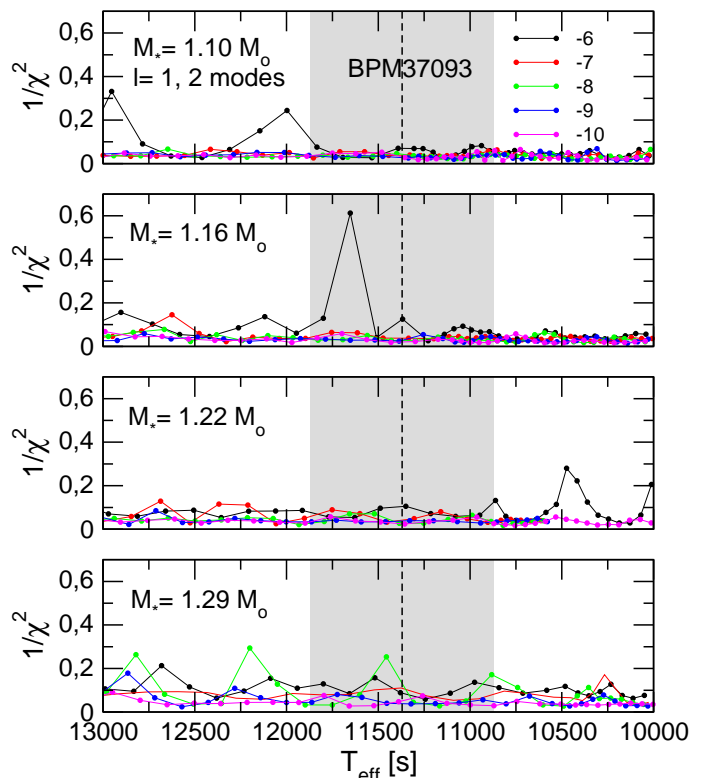
where  $S_0 \equiv \chi^2(M_{\star}^0, M_{\text{H}}^0, T_{\text{eff}}^0)$  is the minimum of  $\chi^2$  which is reached at  $(M_{\star}^0, M_{\text{H}}^0, T_{\text{eff}}^0)$  corresponding to the best-fit model, and  $S$  is the value of  $\chi^2$  when we change the parameter  $i$  (in this case,  $M_{\star}$ ,  $M_{\text{H}}$ , or  $T_{\text{eff}}$ ) by an amount  $d_i$ , keeping fixed the other parameters. The quantity  $d_i$  can be evaluated as the minimum step in the grid of the parameter  $i$ . We obtain the following uncertainties:  $\sigma_{M_{\star}} \sim 0.014M_{\odot}$ ,  $\sigma_{M_{\text{H}}} \sim 6.3 \times 10^{-7}M_{\star}$ , and  $\sigma_{T_{\text{eff}}} \sim 40$  K. The uncertainty in  $L_{\star}$  is derived from the width of the maximum in the function  $(1/\chi^2)$  in terms of  $L_{\star}$ . We obtain  $\sigma_{L_{\star}} \sim 5.8 \times 10^{-4}L_{\odot}$ . The uncertainties in  $R_{\star}$  and  $g$  are derived from the uncertainties in  $M_{\star}$ ,  $T_{\text{eff}}$ , and  $L_{\star}$ .

Table 2 includes the parameters of the best-fit model along with the uncertainties derived above. These are formal uncertainties related to the process of searching for the asteroseismological model, and therefore they can be considered as *internal* uncertainties inherent to the asteroseismological process.

#### 4.5. Asteroseismological distance

We employ the effective temperature and gravity of our best-fit model to infer the absolute  $G$  magnitude ( $M_G$ ) of BPM 37093 in the *Gaia* photometry (D. Koester, private communication). We find  $M_G = 13.53$  mag. On the other hand, we obtain the apparent magnitude  $m_G = 13.8$  mag from the *Gaia* Archive<sup>3</sup>. According to the well-known expression  $\log d = (m_G - M_G + 5)/5$ , we obtain  $d = 11.38 \pm 0.06$  pc and a parallax  $\pi = 87.87 \pm 0.40$  mas. These asteroseismological distance and parallax are somewhat different as compared with those provided directly by *Gaia*, that is,  $d = 14.81 \pm 0.01$  pc and  $\pi = 67.52 \pm 0.04$  mas. However, we note that the uncertainties in the asteroseismological distance

<sup>3</sup> (<https://gea.esac.esa.int/archive/>).



**Fig. 7.** The inverse of the quality function of the period fit in the case in which we allow the periods to be associated to  $\ell = 1$  and  $\ell = 2$  modes in terms of the effective temperature for the ultra-massive DA WD model sequences with different stellar masses ( $M_{\star}$ ) and H envelope thicknesses [ $\log(M_{\text{H}}/M_{\star})$ ], as indicated. The vertical dashed line and the gray strip correspond to the spectroscopic effective temperature of BPM 37093 and its uncertainties ( $T_{\text{eff}} = 11\,370 \pm 500$  K). Note the strong maximum in  $(\chi^2)^{-1}$  for  $M_{\star} = 1.16M_{\odot}$  and  $\log(M_{\text{H}}/M_{\star}) = -6$  at  $T_{\text{eff}} \sim 11\,650$  K. This corresponds to our "best-fit" model (see text for details).

and parallax come mainly from the uncertainties in the effective temperature and the logarithm of the gravity of the best-fit model ( $\sim 40$  K and  $\sim 0.025$ ), which are admittedly small because they are just internal errors. Realistic estimates of these errors are probably much higher (see above Section). That said, we believe that with more realistic estimates of the uncertainties in  $T_{\text{eff}}$  and  $\log g$ , and thus in the errors in the asteroseismological distance and parallax, the agreement with the astrometric values could substantially improve.

#### 4.6. Rotation period

If the stellar rotation is slow and rigid, the rotation frequency  $\Omega$  of the WD is connected with the frequency splitting  $\delta\nu$  through the coefficients  $C_{k,\ell}$ —that depend on the details of the stellar structure—and the values of  $m$  ( $-\ell, \dots, -1, 0, +1, \dots, +\ell$ ), by means of the expression  $\delta\nu = m(1 - C_{k,\ell})\Omega$  (Unno et al. 1989). The period at 564.1 s in Table 1 is actually the average of two very close observed periods which are assumed to be the components  $m = -1$  (562.6 s) and  $m = +1$  (565.5 s) of a rotationally split  $\ell = 2$  mode (see Nitta et al. 2016). Here, it is assumed that the remainder components of the quintuplet ( $m = -2, 0, +2$ ) are not visible for some unknown reason. Under this hypothesis, we derive a frequency splitting of  $\delta\nu = 4.55\mu\text{Hz}$ . Making the same assumption for the pair of observed periods at 633.5 s and 636.7 s (see Nitta et al. 2016), which, averaged, give the period 635.1



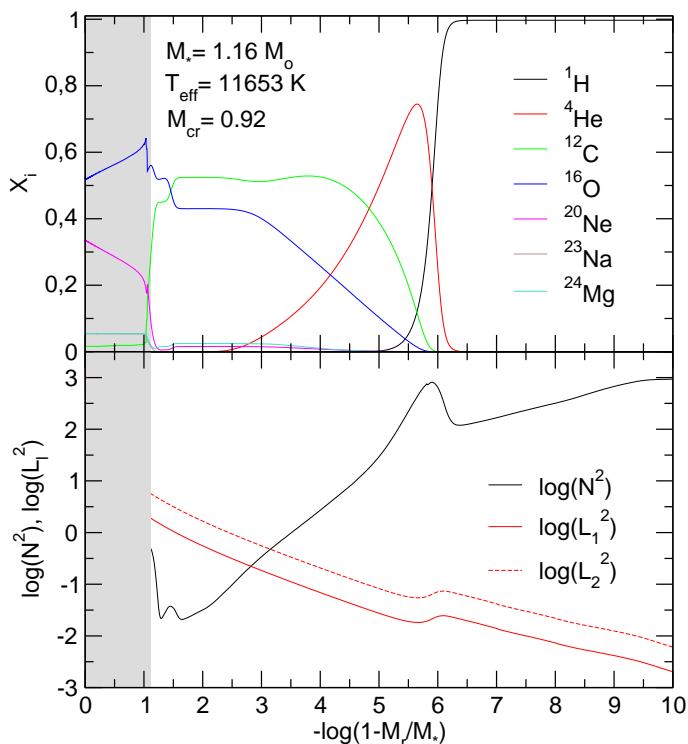


**Fig. 8.** The internal chemical structure (upper panel), and the squared Brunt-Vaisälä and Lamb frequencies for  $\ell = 1$  and  $\ell = 2$  (lower panel) corresponding to our best-fit ultra-massive DA WD model for BPM 37093 with a stellar mass  $M_* = 1.16 M_\odot$ , an effective temperature  $T_{\text{eff}} = 11\,653\text{ K}$ , a H envelope mass of  $\log(M_{\text{H}}/M_*) \sim -6$ , and a crystallized mass fraction of  $M_{\text{cr}} = 0.92M_*$ .

s in Table 1), we have  $\delta\nu = 3.95\mu\text{Hz}$ . For our best-fit model for BPM 37093, we find that the 564 s and 635 s modes have  $C_{k,\ell=2} \sim 0.166$ . Using this value for  $C_{k,\ell}$ , and the averaged frequency splitting,  $\overline{\delta\nu} = 4.25\mu\text{Hz}$ , we obtain a rotation period of  $\sim 55\text{ h}$ . This rotation period is consistent with the rotation-period values inferred from asteroseismology for WD stars (see Table 10 of Córscico et al. 2019). We also can estimate what the rotation period would be if these periods were the components  $m = -1$  and  $m = +1$  of  $\ell = 1$  modes instead of  $\ell = 2$  modes. In that case, we would have  $C_{k,\ell=2} \sim 0.498$  from the best-fit model, and then the rotation period should be of  $\sim 33\text{ h}$ .

#### 4.7. Comparison with previous analyses

Metcalf et al. (2004) carried out a parametric asteroseismological analysis on BPM 37093 on the basis of the eight periods listed in the first column of Table 1. These authors employed DA WD models characterized by chemical transition regions resulting from the assumption of diffusive equilibrium. The free parameters of the analysis are the crystallized mass fraction (that is, the location of the inner boundary conditions for the pulsations, which coincides with the liquid/solid interface), the He and H envelope thickness, and the effective temperature. The authors consider pure C- and O-core WDs, and three fixed stellar-mass values. They obtain a family of asteroseismological models characterized by different stellar parameters, but all of them with 90 % of the mass crystallized. A second parametric asteroseismological analysis of BPM 37093 was performed independently by Brassard & Fontaine (2005), who employed DA WD models with some improved aspects; for example, updated

opacities, chemical transitions resulting from time-dependent element diffusion, and cores made of CO in addition to pure C and O cores. In addition, the models of Brassard & Fontaine (2005) do not consider the crystallized mass fraction as a free parameter, but instead, the value is fixed for each model and results from the predictions of the EoS. The results of this analysis largely differ from those of Metcalfe et al. (2004). Indeed, Brassard & Fontaine (2005) found a set of optimal asteroseismological models characterized by a percentage of crystallized mass in the range 32-82 %. These authors emphasize that the information contained in the eight periods employed in both analyses is not enough to unravel the core chemical structure nor to derive the percentage of crystallized mass of this star, due to the fact that the modes are characterized by high radial orders and therefore, they are in the asymptotic regime of  $g$ -mode pulsations. The strong differences of the results of the works by Metcalfe et al. (2004) and Brassard & Fontaine (2005) could be due to the fact that Metcalfe et al. (2004) only varied the crystallized mass fraction in increments of 10 % (i.e., 10%, 20%, 30%, ..., 80%, 90%). Using a finer grid in the increments of the crystallized mass fraction could result in many other possible best-fit solutions, potentially more in agreement with the larger set of solutions found by Brassard & Fontaine (2005).

The DA WD models employed in the present paper are substantially different as compared with those employed by Metcalfe et al. (2004) and Brassard & Fontaine (2005), particularly regarding the core chemical structure and composition. In fact, while those authors consider cores made of pure C, pure O, and mixtures of 50 % of C and 50 % of O, in the present analysis we consider cores made of O and Ne with evolving chemical structures as predicted by fully evolutionary computations. In addition, our asteroseismological approach, which is based on fully evolutionary models, largely differs from that adopted in the mentioned works, that is, the employment of structure models with a number of adjustable free parameters to search for the optimal asteroseismological models. For these reasons, a direct comparison of our results with those of Metcalfe et al. (2004) and Brassard & Fontaine (2005) is not possible. However, we can emphasize that our analysis favours a WD model with a large fraction of mass in solid phase ( $\sim 92\%$ ), more in line with the results of Metcalfe et al. (2004). Also, the identification of the harmonic degree  $\ell$  and the radial order  $k$  of the pulsation modes for the asteroseismological solutions are similar. Indeed, our analysis predicts that most of the modes are quadrupole modes, except the modes with periods at 531.1 s and 613.5 s, which are dipole modes. In the case of Metcalfe et al. (2004), most of the modes are  $\ell = 2$ , except modes with periods 582.0 s and 613.5 s which are  $\ell = 1$  modes. Finally, Brassard & Fontaine (2005) predict that most of the modes are  $\ell = 2$ , except the mode with periods 613.5 s, which is a  $\ell = 1$  mode. Regarding the radial order of the modes, in our case we obtain  $29 \leq k \leq 36$ , whereas both Metcalfe et al. (2004) and Brassard & Fontaine (2005) analyses predict  $28 \leq k \leq 35$ . The surprising agreement of the identification of the radial order  $k$  of the modes according to Metcalfe et al. (2004) and Brassard & Fontaine (2005) as compared with the current analysis (differing only by 1) could be due to the fact that our best-fit model for BPM 37093 has a large fraction of mass crystallized, so that  $g$ -mode pulsations are insensitive to the ONe-core chemical features, and thus, the pulsational properties of the model resemble those of a model with a similar mass but with a CO core.

**Table 3.** The independent frequencies in the data of GD 518 from Hermes et al. (2013) along with the theoretical periods, harmonic degrees, radial orders, and period differences of the best-fit model.

$\Pi^0$ [sec]	$\nu$ [ $\mu$ Hz]	$\Pi^1$ [sec]	$\ell$	$k$	$\delta_i$ [sec]
$440.2 \pm 1.5$	$2271.7 \pm 7.6$	439.55	2	29	0.70
$513.2 \pm 2.4$	$1948.6 \pm 9.2$	514.10	2	34	-0.90
$583.7 \pm 1.5$	$1713.3 \pm 4.5$	583.09	1	22	0.61

**Table 4.** Same as Table 2, but for GD 518.

Quantity	Spectroscopy	Asteroseismology
$T_{\text{eff}}$ [K]	$12030 \pm 210^{(a)}$	$12060 \pm 38$
$M_{\star}/M_{\odot}$	$1.198^{(b)}$	$1.22 \pm 0.03$
$\log g$ [cm/s <sup>2</sup> ]	$9.08 \pm 0.06^{(a)}$	$9.15 \pm 0.021$
$\log(L_{\star}/L_{\odot})$	—	$-3.34 \pm 0.01$
$\log(R_{\star}/R_{\odot})$	—	$-2.31 \pm 0.008$
$\log(M_{\text{H}}/M_{\star})$	—	$-6 \pm 0.24$
$\log(M_{\text{He}}/M_{\star})$	—	-4
$M_{\text{cr}}/M_{\star}$	$0.955^{(b)}$	0.971
$X_{16\text{O}}$ cent.	—	0.53
$X_{20\text{Ne}}$ cent.	—	0.32

Quantity	Astrometry ( <i>Gaia</i> )	Asteroseismology
$d$ [pc]	$64.57 \pm 0.3$	$49.80 \pm 0.06$
$\pi$ [mas]	$15.48 \pm 0.08$	$20.08 \pm 0.03$

References: (a) Hermes et al. (2013); (b) Camisassa et al. (2019)

## 5. Other ultra-massive ZZ Ceti stars

There are three other pulsating ultra-massive ZZ Ceti stars known to date, apart from BPM 37093. They are GD 518, SDSS J084021.23+522217.4, and J212402.03-600100.0. In contrast to BPM 37093, these three stars show only a few pulsation periods (see Tables 3, 5, and 7), which prevent us from finding a period spacing for these stars. Also, the scarcity of periods inhibits us from carrying out a detailed asteroseismological analysis as in the case of BPM 37097. Then, we will limit ourselves to perform a preliminary analysis of period-to-period fits for GD 518 and SDSS J084021.23+522217.4. The star J212402.03-600100.0 is excluded from this analysis because it only has a single detected period.

### 5.1. GD 518

Pulsations in WD J165915.11+661033.3 (GD 518) were first detected by Hermes et al. (2013). Model-atmosphere fits to this star indicate that it is located in the ZZ Ceti instability strip with  $T_{\text{eff}} \sim 12030$  K and  $\log g \sim 9.08$ , which would correspond to a mass of  $1.20M_{\odot}$  if the ONe-core WD models from Althaus et al. (2005a) are used, or  $1.23M_{\odot}$  if the CO-core WD models from Wood (1995) are employed. The value of the stellar mass of the star is  $M_{\star} = 1.198M_{\odot}$  if the evolutionary tracks of ONe-core WD models of Camisassa et al. (2019) are adopted. To date, no asteroseismological analysis has been performed to this star. Our period-to-period fits for this star indicate that our best fit model—the one which minimizes the merit function from Eq. (3)—is characterized by a value of  $\chi^2 = 0.56$ ,  $\bar{\delta} = 0.74$  s,  $\sigma = 0.75$  s, and  $\text{BIC} = 0.22$ , and has a stellar mass of  $1.22M_{\odot}$  and  $T_{\text{eff}} = 12060$  K (see Table 4 and Fig. 9). The stellar mass of the asteroseismological model is consistent with the spectroscopic mass derived from the evolutionary tracks of Camisassa et al. (2019).

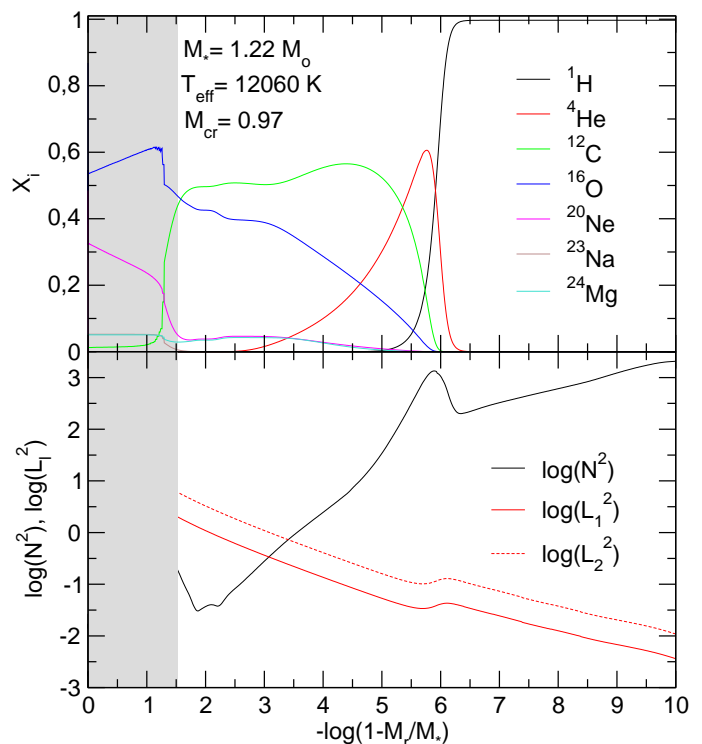


**Fig. 9.** Same as in Fig. 8, but for the asteroseismological best-fit model of GD 518.

The asteroseismological distance and parallax inferred for GD 518, derived in the same way than for BPM 37093, are  $d = 49.80 \pm 0.06$  pc and  $\pi = 20.08 \pm 0.03$  mas. These values are somewhat different than those provided by *Gaia*, that is,  $d = 64.57 \pm 0.3$  pc and  $\pi = 15.48 \pm 0.08$  mas. The agreement between these sets of values could improve if we could employ more realistic values for the uncertainties in  $T_{\text{eff}}$  and  $\log g$  of the asteroseismological model for GD 518, in a similar way than for BPM 37093 (see discussion at the end of Sect. 4.5).

### 5.2. SDSS J084021.23+522217.4

This ultra-massive ZZ Ceti star was discovered by Curd et al. (2017) from a sample of DA WD from the SDSS DR7 and DR10. Model-atmosphere fits indicate  $T_{\text{eff}} \sim 12160$  K,  $\log g \sim 8.93$  and  $M_{\star} \sim 1.16M_{\odot}$ . These results are in good agreement with the preliminary asteroseismological analysis performed by the same authors, where their best-fit CO-core WD model has  $M_{\star} = 1.14M_{\odot}$ ,  $M_{\text{H}} = 5.8 \times 10^{-7}M_{\star}$ ,  $M_{\text{He}} = 4.5 \times 10^{-4}M_{\star}$ ,  $0.50 \leq M_{\text{cr}}/M_{\star} \leq 0.70$  and  $11850 \leq T_{\text{eff}} \leq 12350$  K.

Our best fit model is characterized by  $\chi^2 = 0.14$ ,  $\bar{\delta} = 0.37$  s,  $\sigma = 0.38$  s, and  $\text{BIC} = -0.37$  with one period (797.4 s) identified as a  $\ell = 2$  mode, and the remaining periods identified as  $\ell = 1$  modes. The derivation of the stellar parameters gives  $T_{\text{eff}} = 12550$  K,  $M_{\star} = 1.10M_{\odot}$ ,  $M_{\text{H}}/M_{\star} = 1.02 \times 10^{-7}$ ,  $M_{\text{He}}/M_{\star} = 3.0 \times 10^{-4}$ ,  $M_{\text{cr}}/M_{\star} = 0.81$ , with a central  $^{20}\text{Ne}$  abundance of 0.52. The stellar mass derived from the asteroseismological model is somewhat smaller than the value derived spectroscopically on the basis of the evolutionary tracks of Camisassa et al. (2019). On the other hand, the disagreement regarding the mass of the crystallized part of the core as compared with the result found by Curd et al. (2017) is because here we are employing ONe-core WD models, whereas those authors consider CO-core WD models. When searching for the best-fit

**Table 5.** The independent frequencies in the data of SDSS J084021.23+522217.4 from Curd et al. (2017) along with the theoretical periods, harmonic degrees, radial orders, and period differences of the best-fit model.

$\Pi^O$ [sec]	$\nu$ [ $\mu$ Hz]	$\Pi^T$ [sec]	$\ell$	$k$	$\delta_i$ [sec]
$172.7 \pm 0.4$	5790.4	172.23	1	3	0.47
$326.6 \pm 1.3$	3061.8	326.88	1	8	-0.28
$797.4 \pm 8.0$	1254.14	797.76	2	40	-0.36

**Table 6.** Same as Table 2, but for SDSS J084021.23+522217.4.

Quantity	Spectroscopy	Asteroseismology
$T_{\text{eff}}$ [K]	$12\,160 \pm 320^{(a)}$	$12\,550 \pm 70.$
$M_{\star}/M_{\odot}$	$1.139^{(b)}$	$1.10 \pm 0.04$
$\log g$ [ $\text{cm/s}^2$ ]	$8.93 \pm 0.07^{(a)}$	$8.84 \pm 0.02$
$\log(L_{\star}/L_{\odot})$	—	$-3.02 \pm 0.01$
$\log(R_{\star}/R_{\odot})$	—	$-2.18 \pm 0.005$
$\log(M_{\text{H}}/M_{\star})$	—	$-7 \pm 0.21$
$\log(M_{\text{He}}/M_{\star})$	—	-3.5
$M_{\text{cr}}/M_{\star}$	$0.945^{(b)}$	0.813
$X_{16\text{O}}$ cent.	—	0.52
$X_{20\text{Ne}}$ cent.	—	0.31

Quantity	Astrometry ( <i>Gaia</i> )	Asteroseismology
$d$ [pc]	$138.50 \pm 4.0$	$89.95 \pm 0.08$
$\pi$ [mas]	$7.22 \pm 0.21$	$11.12 \pm 0.01$

References: (a) Curd et al. (2017); (b) Camisassa et al. (2019)

**Table 7.** The single frequency in the data of WD J212402.03–600100.0 from Rowan et al. (2019).

$\Pi^O$ [sec]	$f$ [ $\mu$ Hz]
357	2801

model with all periods assumed to be associated to  $\ell = 1$  modes, we found the same best-fit model as in the previous analysis, but with a poorer quality function ( $\chi^2 = 1.56$ ).

The asteroseismological distance and parallax inferred for this star are  $d = 89.95 \pm 0.08$  pc and  $\pi = 11.12 \pm 0.01$  mas, which differ from the *Gaia* values,  $d = 138.50 \pm 4.0$  pc and  $\pi = 7.22 \pm 0.21$  mas. Again, a better estimate of the uncertainties of the effective temperature and gravity of the asteroseismological model could contribute to bring the asteroseismological distance and parallax values closer to those derived by *Gaia*.

### 5.3. WD J212402

The variability of WD J212402 was discovered by Rowan et al. (2019) from time-series GALEX space-telescope observations. This star has  $T_{\text{eff}} = 12\,510$  K and  $\log g = 8.98$  (Gentile Fusillo et al. 2019). The stellar mass of the star is  $M_{\star} = 1.16M_{\odot}$  and the crystallized mass fraction should be of  $M_{\text{cr}}/M_{\star} \sim 0.90$  according to the evolutionary tracks of Camisassa et al. (2019). Unfortunately, only a single period has been detected (Table 7), preventing us from attempting an asteroseismological analysis. It would be very important to have additional observations of this star to detect more pulsation periods.

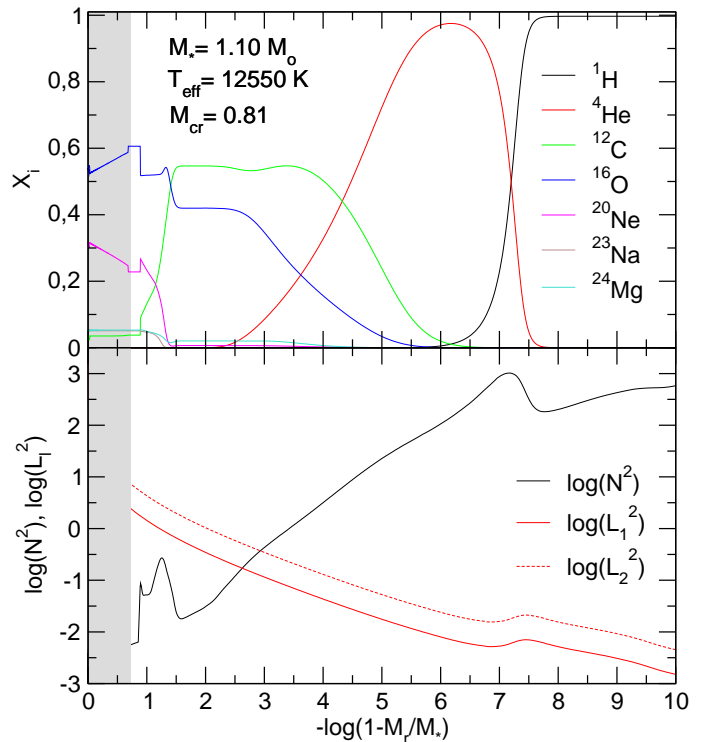


**Fig. 10.** Same as in Fig. 8, but for the asteroseismological best-fit model of SDSS J084021.23+522217.4.

## 6. Summary and conclusions

In this paper, we have conducted for the first time an asteroseismological study of the ultra-massive ZZ Ceti stars known hitherto by employing an expanded set of grid of ONE-core WD models presented in Camisassa et al. (2019). The stellar models on which this study is based consider crystallization with chemical rehomogenization due to phase separation. We have included ultra-massive WD models with different thicknesses of the H envelope, with the aim of expanding the parameter space in our asteroseismological exploration.

For the ultra-massive ZZ Ceti star BPM 37093, we have carried out a detailed asteroseismological analysis that includes the derivation of a mean period spacing of  $\sim 17$  s, which is associated to  $\ell = 2$   $g$  modes. We have not been able, however, to infer the stellar mass of the star by comparing the observed period spacing with the averaged theoretical period spacings. This is due to the intrinsic degeneracy of the dependence of  $\Delta\Pi$  with the three parameters  $M_{\star}$ ,  $T_{\text{eff}}$  and  $M_{\text{H}}$ . On the other hand, we have derived a best-fit model for the star, by considering their individual pulsation periods. This model is characterized by  $T_{\text{eff}} = 11\,650$  K,  $M_{\star} = 1.16M_{\odot}$ ,  $\log(M_{\text{H}}/M_{\star}) = -6$ , and  $M_{\text{cr}}/M_{\star} = 0.92$  (see Table 2). In addition, we have derived an asteroseismological distance of 11.38 pc, which somewhat differs from the astrometric distance measured by *Gaia*, of 14.81 pc. Finally, a rotation period of 55 h has been inferred, under the assumption that the modes that exhibit frequency splittings are associated to  $\ell = 2$  modes. For the ultra-massive ZZ Ceti stars GD 518 and SDSS J084021, which exhibit only three periods, we have performed period-to-period fits, and we find asteroseismological models whose characteristics are listed in Tables 4 and 6. In particular, this analysis predicts that the crystallized mass fraction of these stars are  $M_{\text{cr}}/M_{\star} = 0.97$  (GD 518) and  $M_{\text{cr}}/M_{\star} = 0.81$  (SDSS J084021). The asteroseismological distances inferred for these stars (50 pc and 90 pc, respectively) are

somewhat different to the distances measured by *Gaia* (65 pc and 139 pc, respectively). Finally, for the ultra-massive ZZ ceti star WD J212402, which exhibits one single period, it is not possible to do any kind of asteroseismological inference at this stage.

Tables 2, 4, and 6 include the parameters of the best-fit models for BPM 37093, GD 518, and SDSS J084021.23+522217.4, respectively. We note that for two of the three stars studied, that is BPM 37093 and GD 518, the percentage of crystallization is larger than 90% by mass, which is larger than the mass of the ONe core. Thus, since  $g$ -mode pulsations only sample the non-crystallized regions, and since these regions are dominated by O, C, He and H, it is not surprising that the best-fit seismological models are consistent with prior studies which assumed CO cores, particularly in the case of BPM 37093.

In Tables 2, 4, and 6 we have included the formal uncertainties related to the process of searching for the asteroseismological model, and therefore they can be considered as *internal* uncertainties inherent to the asteroseismological process. An estimation of more realistic uncertainties in the structural quantities that characterize the asteroseismological models of these stars ( $T_{\text{eff}}$ ,  $M_{\star}$ ,  $M_{\text{H}}$ ,  $M_{\text{He}}$ ,  $R_{\star}$ , etc) is very difficult to obtain, since they depend on the uncertainties affecting the physical processes of the progenitor evolution. An estimate of the impact of the uncertainties in the prior evolution on the structural parameters of the asteroseismological models has been carried out by De Gerónimo et al. (2017, 2018) for ZZ Ceti stars of intermediate masses harbouring CO cores. These authors derive typical uncertainties of  $\Delta M_{\star}/M_{\star} \lesssim 0.05$ ,  $\Delta T_{\text{eff}} \lesssim 300$  K and a factor of two in the thickness of the H envelope. While we can not directly extrapolate these results to our analysis of ultra-massive DA WD models with ONe cores, we can adopt them as representative of the real uncertainties affecting the parameters of our asteroseismological models for BPM 37093, GD 518, and SDSS J084021.23+522217.4.

In this paper, we have assumed that ultra-massive WDs ( $M_{\star} \gtrsim 1M_{\odot}$ ) come from single-star evolution and must have ONe cores. However, it cannot be discarded that these objects are the result of mergers of two WDs (the so-called "double degenerate scenario"; see, e.g., García-Berro et al. 2012; Schwab et al. 2012) in a binary system, in which case it is expected that they have CO cores. The study of the evolutionary and pulsational properties of ultra-massive WDs resulting from WD+WD mergers is beyond the scope of the present paper and will be the focus of a future investigation.

We close the article by emphasizing the need of new photometric observations from the ground or from space (e.g., TESS) in order to find more variable ultra-massive WDs, and also to re-observe the already known objects (for instance WD J212402) in order to find more periods. This will result in reliable asteroseismological analyses that could yield valuable information about the crystallization processes in WDs. Also, it could be possible to derive the core chemical composition and, in turn, to infer their evolutionary origin—that is, either single-star evolution or binary-star evolution with the merger of two WDs.

*Acknowledgements.* We wish to acknowledge the suggestions and comments of an anonymous referee that strongly improved the original version of this work. We gratefully acknowledge Prof. Detlev Koester for providing us with a tabulation of the absolute magnitude of DA WD models in the *Gaia* photometry. Part of this work was supported by AGENCIA through the Programa de Modernización Tecnológica BID 1728/OC-AR, and by the PIP 112-200801-00940 grant from CONICET. This research has made use of NASA's Astrophysics Data System.

## References

- Abrikosov, A. A. 1961, *Sov. Phys. JETP*, 12, 1254
- Althaus, L. G., Camisassa, M. E., Miller Bertolami, M. M., Córscico, A. H., & García-Berro, E. 2015, *A&A*, 576, A9
- Althaus, L. G., Córscico, A. H., Bischoff-Kim, A., et al. 2010a, *ApJ*, 717, 897
- Althaus, L. G., Córscico, A. H., Isern, J., & García-Berro, E. 2010b, *A&A Rev.*, 18, 471
- Althaus, L. G., Córscico, A. H., Kepler, S. O., & Miller Bertolami, M. M. 2008, *A&A*, 478, 175
- Althaus, L. G., García-Berro, E., Isern, J., & Córscico, A. H. 2005a, *A&A*, 441, 689
- Althaus, L. G., García-Berro, E., Renedo, I., et al. 2010c, *ApJ*, 719, 612
- Althaus, L. G., Miller Bertolami, M. M., & Córscico, A. H. 2013, *A&A*, 557, A19
- Althaus, L. G., Serenelli, A. M., Panei, J. A., et al. 2005b, *A&A*, 435, 631
- Bischoff-Kim, A., Montgomery, M. H., & Winget, D. E. 2008, *ApJ*, 675, 1505
- Bognár, Z., Páparó, M., Molnár, L., et al. 2016, *MNRAS*, 461, 4059
- Borucki, W. J. 2016, *Reports on Progress in Physics*, 79, 036901
- Bradley, P. A. 1998, *ApJs*, 116, 307
- , 2001, *ApJ*, 552, 326
- Bradley, P. A., Winget, D. E., & Wood, M. A. 1993, *ApJ*, 406, 661
- Brassard, P. & Fontaine, G. 2005, *ApJ*, 622, 572
- Brassard, P., Fontaine, G., Wesemael, F., & Hansen, C. J. 1992a, *ApJS*, 80, 369
- Brassard, P., Fontaine, G., Wesemael, F., & Tassoul, M. 1992b, *ApJS*, 81, 747
- Camisassa, M. E., Althaus, L. G., Córscico, A. H., et al. 2019, *A&A*, 625, A87
- , 2016, *ApJ*, 823, 158
- Camisassa, M. E., Althaus, L. G., Rohrmann, R. D., et al. 2017, *ApJ*, 839, 11
- Castanheira, B. G. & Kepler, S. O. 2008, *MNRAS*, 385, 430
- Córscico, A. H. & Althaus, L. G. 2006, *A&A*, 454, 863
- Córscico, A. H., Althaus, L. G., Benvenuto, O. G., & Serenelli, A. M. 2002, *A&A*, 387, 531
- Córscico, A. H., Althaus, L. G., Miller Bertolami, M. M., & Kepler, S. O. 2019, *A&A Rev.*, 27, 7
- Córscico, A. H., Althaus, L. G., Montgomery, M. H., García-Berro, E., & Isern, J. 2005, *A&A*, 429, 277
- Córscico, A. H., García-Berro, E., Althaus, L. G., & Isern, J. 2004, *A&A*, 427, 923
- Curd, B., Gianninas, A., Bell, K. J., et al. 2017, *MNRAS*, 468, 239
- De Gerónimo, F. C., Althaus, L. G., Córscico, A. H., Romero, A. D., & Kepler, S. O. 2017, *A&A*, 599, A21
- , 2018, *A&A*, 613, A46
- De Gerónimo, F. C., Córscico, A. H., Althaus, L. G., Wachlin, F. C., & Camisassa, M. E. 2019, *A&A*, 621, A100
- Fontaine, G. & Brassard, P. 2008, *PASP*, 120, 1043
- Fu, J.-N., Dolez, N., Vauclair, G., et al. 2013, *MNRAS*, 429, 1585
- García-Berro, E., Lorén-Aguilar, P., Aznar-Siguán, G., et al. 2012, *ApJ*, 749, 25
- García-Berro, E., Torres, S., Althaus, L. G., et al. 2010, *Nature*, 465, 194
- Gentile Fusillo, N. P., Tremblay, P.-E., Gänsicke, B. T., et al. 2019, *MNRAS*, 482, 4570
- Giammichele, N., Charpinet, S., Brassard, P., & Fontaine, G. 2017a, *A&A*, 598, A109
- Giammichele, N., Charpinet, S., Fontaine, G., & Brassard, P. 2017b, *ApJ*, 834, 136
- Handler, G., Pikall, H., O'Donoghue, D., et al. 1997, *MNRAS*, 286, 303
- Hermes, J. J., Kepler, S. O., Castanheira, B. G., et al. 2013, *ApJ*, 771, L2
- Kanaan, A., Kepler, S. O., Giovannini, O., & Diaz, M. 1992, *ApJ*, 390, L89
- Kanaan, A., Nitta, A., Winget, D. E., et al. 2005, *A&A*, 432, 219
- Kanaan, A., Nitta-Kleinman, A., Winget, D. E., et al. 2000, *Baltic Astronomy*, 9, 87
- Kawaler, S. D. 1988, in *IAU Symposium*, Vol. 123, *Advances in Helio- and Asteroseismology*, ed. J. Christensen-Dalsgaard & S. Frandsen, 329
- Kawaler, S. D. & Bradley, P. A. 1994, *ApJ*, 427, 415
- Kepler, S. O., Pelisoli, I., Koester, D., et al. 2016, *MNRAS*, 455, 3413
- Kirzhnits, D. A. 1960, *Sov. Phys. JETP*, 11, 365
- Kleinman, S. J., Kepler, S. O., Koester, D., et al. 2013, *ApJs*, 204, 5
- Koen, C. & Laney, D. 2000, *MNRAS*, 311, 636
- Landolt, A. U. 1968, *ApJ*, 153, 151
- Medin, Z. & Cumming, A. 2010, *Phys. Rev. E*, 81, 036107
- Metcalf, T. S., Montgomery, M. H., & Kanaan, A. 2004, *ApJ*, 605, L133
- Miller Bertolami, M. M. 2016, *A&A*, 588, A25
- Miller Bertolami, M. M., Althaus, L. G., Unglaub, K., & Weiss, A. 2008, *A&A*, 491, 253
- Montgomery, M. H. 1998, PhD thesis, THE UNIVERSITY OF TEXAS AT AUSTIN
- Montgomery, M. H. & Winget, D. E. 1999, *ApJ*, 526, 976
- Nather, R. E., Winget, D. E., Clemens, J. C., Hansen, C. J., & Hine, B. P. 1990, *ApJ*, 361, 309
- Nitta, A. 2000, PhD thesis, The University of Texas at Austin
- Nitta, A., Kepler, S. O., Chené, A.-N., et al. 2016, *IAU Focus Meeting*, 29B, 493
- O'Donoghue, D. 1994, *MNRAS*, 270, 222

- Renedo, I., Althaus, L. G., Miller Bertolami, M. M., et al. 2010, *ApJ*, 717, 183
- Ricker, G. R., Winn, J. N., Vanderspek, R., et al. 2014, in *Proc. SPIE*, Vol. 9143, *Space Telescopes and Instrumentation 2014: Optical, Infrared, and Millimeter Wave*, 914320
- Romero, A. D., Córsico, A. H., Althaus, L. G., et al. 2012, *MNRAS*, 420, 1462
- Romero, A. D., Córsico, A. H., Castanheira, B. G., et al. 2017, *ApJ*, 851, 60
- Romero, A. D., Kepler, S. O., Córsico, A. H., Althaus, L. G., & Fraga, L. 2013, *ApJ*, 779, 58
- Rowan, D. M., Tucker, M. A., Shappee, B. J., & Hermes, J. J. 2019, *MNRAS*, 486, 4574
- Salpeter, E. E. 1961, *ApJ*, 134, 669
- Schwab, J., Shen, K. J., Quataert, E., Dan, M., & Rosswog, S. 2012, *MNRAS*, 427, 190
- Siess, L. 2010, *A&A*, 512, A10
- Tassoul, M., Fontaine, G., & Winget, D. E. 1990, *ApJs*, 72, 335
- Tremblay, P.-E., Fontaine, G., Fusillo, N. P. G., et al. 2019, *Nature*, 565, 202
- Unno, W., Osaki, Y., Ando, H., Saio, H., & Shibahashi, H. 1989, *Nonradial oscillations of stars*
- Van Cleve, J. E., Howell, S. B., Smith, J. C., et al. 2016, *PASP*, 128, 075002
- van Horn, H. M. 1968, *ApJ*, 151, 227
- Wachlin, F. C., Miller Bertolami, M. M., & Althaus, L. G. 2011, *A&A*, 533, A139
- Winget, D. E. & Kepler, S. O. 2008, *ARA&A*, 46, 157
- Winget, D. E., Kepler, S. O., Campos, F., et al. 2009, *ApJ*, 693, L6
- Winget, D. E., Kepler, S. O., Kanaan, A., Montgomery, M. H., & Giovannini, O. 1997, *ApJ*, 487, L191
- Wood, M. A. 1995, in *Lecture Notes in Physics*, Berlin Springer Verlag, Vol. 443, *White Dwarfs*, ed. D. Koester & K. Werner, 41
- York, D. G., Adelman, J., Anderson, Jr., J. E., et al. 2000, *AJ*, 120, 1579
- Zhang, E. H., Robinson, E. L., & Nather, R. E. 1986, *ApJ*, 305, 740